
A novel hybrid system with RC-encased steel joists

Claudio Amadio* — **Lorenzo Macorini**** — **Sveva Sorgon***
Giuseppe Suraci***

* *Department of Civil and Environmental Engineering, University of Trieste
Pl. le Europa 1, 34127 Trieste, Italy
amadio@units.it; ing.sorgon@libero.it*

** *Department of Civil and Environmental Engineering, Imperial College London
South Kensington Campus, SW7 2AZ, London, UK
l.macorini@imperial.ac.uk*

*** *Studio Suraci, Udine, Italy
suraci.giuseppe@studiosuraci.it*

ABSTRACT. The paper presents the main results of an experimental and numerical study on a novel structural frame system, which employs RC encased steel joist beams and columns. An accurate 3D numerical model has been used to represent the resistance mechanisms in beams and beam-to-column connections. Experimental and numerical outcomes have been employed to develop suitable analytical models to be used in practical design. In particular, the beam flexural response has been investigated, providing a simple relationship for the flexural rigidity at different load levels. Capacity models have been then proposed for the bending and shear resistance of partially and fully-encased beams, and for exterior beam-to-column joints.

RÉSUMÉ. Cet article présente les principaux résultats d'une étude numérique et expérimentale effectuée sur un nouveau système structural qui utilise des poutres et des colonnes constituées d'éléments en treillis d'acier revêtues de béton. On utilise un modèle 3D particulièrement soigné pour représenter les mécanismes résistants dans les poutres et dans les connexions poutre-colonne. Les résultats numériques et expérimentaux servent à développer un modèle analytique approprié, utilisable dans la pratique projectuelle. On étudie notamment la réponse flexionnelle des poutres en fournissant une relation simple pour la rigidité flexionnelle en fonction de différents niveaux de chargement. On propose ensuite des modèles pour évaluer la résistance à la flexion et au cisaillement de poutres partiellement ou entièrement revêtues et pour les joints externes poutre-colonne.

KEYWORDS: composite structures, RC encased steel joist, beam-to-column connections, shear resistance mechanism, analytical models for shear and bending resistance.

MOTS-CLÉS: structures composites, poutres en treillis d'acier revêtues de béton, connexions poutre-colonne, mécanismes résistant au cisaillement, modèles analytiques pour la résistance à la flexion et au cisaillement.

DOI:10.3166/EJECE.15.1433-1463 © 2011 Lavoisier, Paris

1. Introduction

The paper investigates a new frame structural solution with reinforced concrete (RC) encased steel joists. This represents an advanced steel-concrete composite system, which can be used also to resist earthquake loading. It assures performance not only higher than simple RC and steel frames, but in some aspects, also superior than traditional steel-concrete composite structures.

In the past, a significant research effort has been devoted to develop steel-concrete composite systems. A large number of experimental tests and numerical investigations have been carried out on composite beams, columns and beam-to-column connections, analysing specific resistance mechanisms and structural performance. Simple analytical methods for traditional steel-concrete composite beams and columns (Johnson, 1994), where the interaction between RC member and steel profile relies mainly on mechanical shear connection devices, have been developed for practical design and included in codes of practice (e.g. Eurocode 4, CEN 2004). Thus, at present, traditional composite beams and columns are more and more frequently employed in multi-storey buildings and in girder bridges. The effective combination of steel and concrete, allows the most favourable use of the mechanical and physical properties of the two materials. Structural steel is mainly used to resist tensile and shear stresses, while concrete to withstand compression forces. Moreover, in partially and fully encased composite columns, concrete prevents local buckling in relatively thin steel plates under compression, and assures an effective protection against fire.

The use of composite sections, where steel profile is embedded in concrete, represents an optimal solution when designing multi-storey medium- high-rise buildings. As it allows the floor-to-floor height, and the overall size of vertical elements to be minimized. This has driven the research towards the investigation of more advanced steel-concrete composite structures, as the slim floor (Mullett, 1998) and the girder-slab (Naccarato, 2000) systems. Both solutions guarantee also adequate fire protection, but are not suitable for moment-resisting frames, as they employ pinned beam-to-column connections. Other studies have addressed the use of new steel-concrete composite solutions for unrestrained frames (Ju *et al.*, 2007), even to resist earthquake loading (Parra-Montesinos *et al.*, 2005). Most of the new advanced composite systems use steel truss embedded in RC for beams and columns. They do not require any shear connection to transfer stresses from steel components to RC, and employ only steel-to-steel connections for member and beam-to-column joints. The use of RC-embedded steel joist has been proved to be the most effective solution to withstand high flexural and shear forces, with a favourable span-to-depth ratio, and to build practical continuous beam-to-column joints. Specific studies have been devoted to determine suitable structural arrangements to resist shear (Khuntia and Goel, 1999a; 1999b) and torsion (Hsu *et al.*, 2004), which represent the most critical failure mechanisms, difficult to be represented using simple analytical models. Conversely, flexural capacity is usually easy to be determined, especially when the steel

components are fully encased in concrete, as local buckling is prevented. Experimental outcomes (Khuntia and Goel 1999a) have also confirmed the effectiveness of using fibre reinforced concrete (FRC) to resist shear, and also that arrangements with diagonal web bars provide high shear capacity, while the use of vertical bars does not guarantee adequate performance.

In general, to date valuable results have been achieved in the analysis of advanced steel-concrete composite systems. New structural solutions have been developed and their performance has been checked in several experimental tests and by means of numerical analyses. However more research is needed, especially to determine resistance mechanisms for FRC- and RC-encased steel joist components, thus leading to the formulation of sound analytical capacity models to be used in practical design.

In this research, the main resistance mechanisms of a novel frame hybrid system with RC-encased steel joist have been investigated by using results of experimental tests and accurate nonlinear numerical simulations. In the following, after presenting the analysed structural solution, some experimental outcomes and the main characteristics of the 3D nonlinear numerical models, which have been employed in the analyses, will be shown. Finally, specific analytical models to be used in structural design will be presented. They have been purposely developed to determine flexural and shear capacity of beams and beam-to-column joints with RC-encased steel joist.

2. Hybrid system with RC-encased steel joist members

In the analysed structural system, RC-encased steel joist beams and columns are used to form unrestrained frames, which resist vertical and horizontal forces. When hybrid frames are employed to withstand seismic loading, beam-to-column connections are designed to dissipate the energy provided by earthquake through plastic deformation. The characteristic steel joist used for beams and columns, corresponds to a steel box truss. It is made of two steel trusses, which are formed by a pair of top angles laced to a pair of bottom angles through serpentine steel bars (web diagonal bars). The two parallel steel trusses are then connected by means of horizontal bars, forming a box (Figure 1).

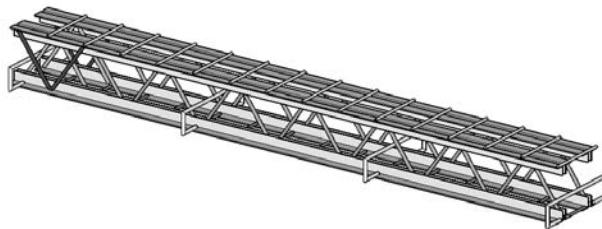


Figure 1. Steel box truss for RC-encased steel joist beams

The hybrid element can be either fully or partially prefabricated. The former case is typical for columns, while the latter for beams, where usually the top concrete is cast in place to connect the beam to the floor and to the column (Figure 2). All the connections between the different structural components are steel-to-steel connections. Therefore the traditional assembling techniques for steel structures can be easily used. As in the case of the beam-to-column joints, where four steel plates set in the column at the joint region (Figure 3), are welded in situ to the top and bottom steel angles of the hybrid beam, so as to guarantee continuity between column and beam, also before the concrete hardening.

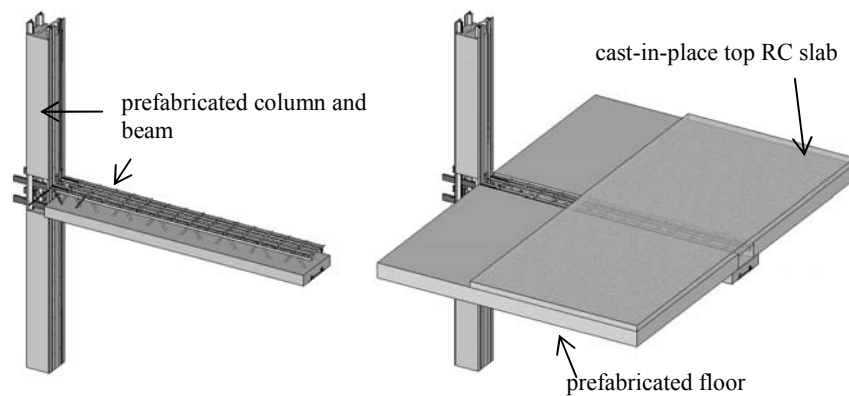


Figure 2. *RC-encased steel joist beam and column and floor system*

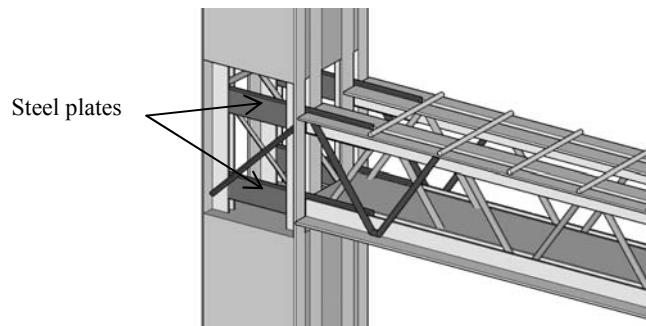


Figure 3. *Beam-to-column connection for RC-encased steel joist elements*

The developed structural frame solution guarantees high construction speed, as it does not require formwork for the erection. Before the hardening of the cast-in-place concrete, the beam, formed by the steel joist and the bottom part of RC member, must be able to transfer its weight and the weight of the floor to the column, without using intermediate removable props. Therefore, in structural design, it is important

to check not only the capacity of the structural system at serviceability and collapse, but also during the construction, when the beam cross section is characterised by a reduced shear and bending resistance, because of the lack of the top RC.

3. Experimental tests

In order to investigate the actual response of RC-encased steel joist members and connections, two beams and an external beam-to-column joint were tested to collapse (Amadio *et al.*, 2008). The two beams, hereinafter referred to as beams A and B (Figure 4), are 6 m long and correspond to a partially encased and a fully encased member respectively. They are representative of a hybrid structure which carries the loads during the construction (beam A) and in service (beam B), after the cast-in-place concrete hardening. For convenience in beam-to-column joint test set-up, the hybrid column was not pre-stressed to simulate internal axial force due to floor loads. However, more tests are planned to investigate the joint performance, considering different levels of axial force in the column.

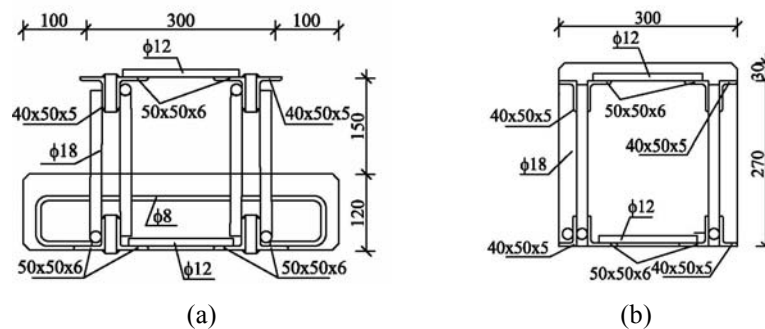


Figure 4. Cross section of the beams A (a) and B (b) (all dimensions in [mm])

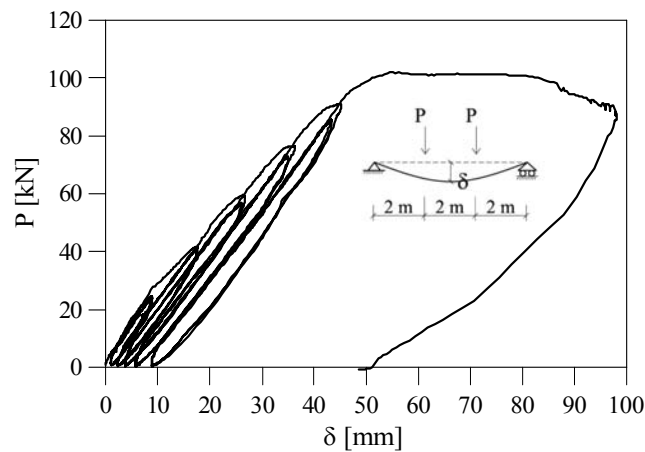
Geometrical characteristics and a detailed description of the tests set-up can be found in Amadio *et al.*, 2008. As far as material properties are concerned, concrete mean compressive and tensile strength, f_{cm} and f_{ctm} respectively, were determined in tests on cubes and through Brazilian cylinder splitting tests and are reported in Table 1. While mean yield strength $f_{ys} = 422$ MPa, ultimate strength $f_{us} = 568$ MPa and a maximum elongation of 28% were obtained in tensile tests on structural steel.

In the tests on beams and beam-to-column connection, displacements, rotations and local deformation in steel components (angles and bars) were measured (Amadio *et al.*, 2008). In particular, in the test on beam-to-column connection, the joint rotation was determined considering the horizontal displacements at the top and bottom of the joint region, which were measured using linear variable displacement transducers (LVDT).

Table 1. Mechanical properties of concrete

Specimen	f_{cm} [MPa]	f_{ctm} [MPa]
Beam A	50.9	4.15
Beam B	44.7	4.16
Joint	45.6	4.78

Figure 5 shows the experimental curve for beam A, where point load P , which is half of the total load on the beam, is plotted against vertical displacement at mid-span δ . The beam collapsed under four-point load bending (Figure 6), because of buckling in the top steel angles (Figure 7). However, the plastic bending capacity was reached before collapse, as plastic deformation was measured in the top and bottom angles at mid-span. Conversely, maximum strain in web diagonal bars was less than the yielding value. Figure 8 displays external load P against vertical displacement at mid span δ measured in the four-point load bending test for beam B (Figure 9). The beam B response is characterised by higher ductility than beam A. In this case, collapse occurred when the top concrete crushed and split off at mid-span (Figure 10), while local buckling in steel components under compression was prevented by surrounding concrete. Plastic deformation was observed only in the bottom steel angles, while top angle and web diagonal bars remained elastic.

**Figure 5.** Force-maximum displacement curve for type A beam

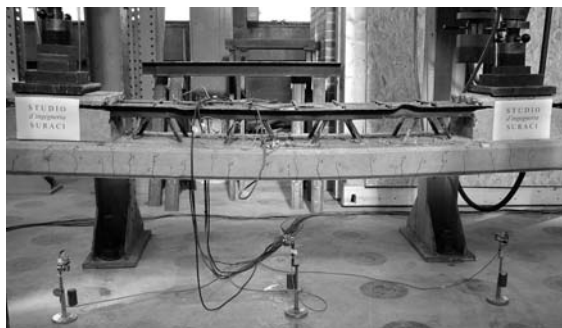


Figure 6. *Beam type A under four-point load bending*



Figure 7. *Local buckling in the top angles at collapse*

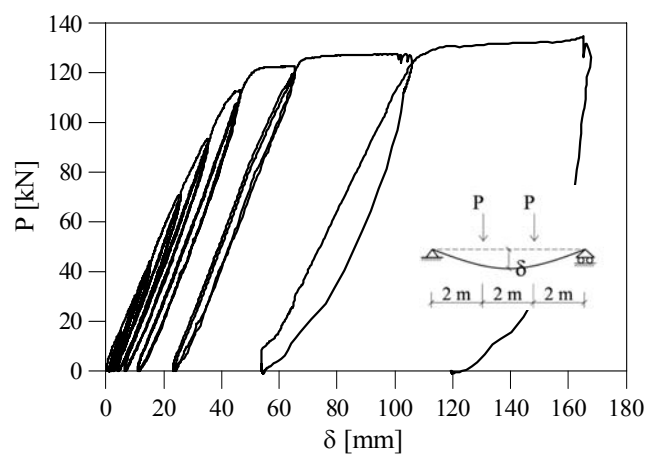


Figure 8. *Force-maximum displacement experimental curve for type B beam*



Figure 9. *Beam type B under four-point load bending*

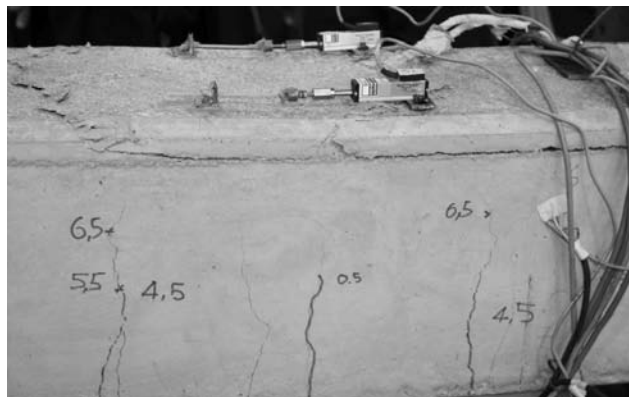


Figure 10. *Concrete split off at collapse*

Finally, the force-rotation curve, obtained in the experimental test for the hybrid beam-to-column connection is shown in Figure 11. A full scale joint specimen (Figure 12), made up of a column 3.8 m high, simple supported at the two ends and connected to a cantilever beam 2.0 m long, was tested by applying a vertical force P at the end of the cantilever.

Figure 13 displays damage in the joint region during the tests. More details on the test set-up and experimental results can be found in Amadio *et al.* (2008).

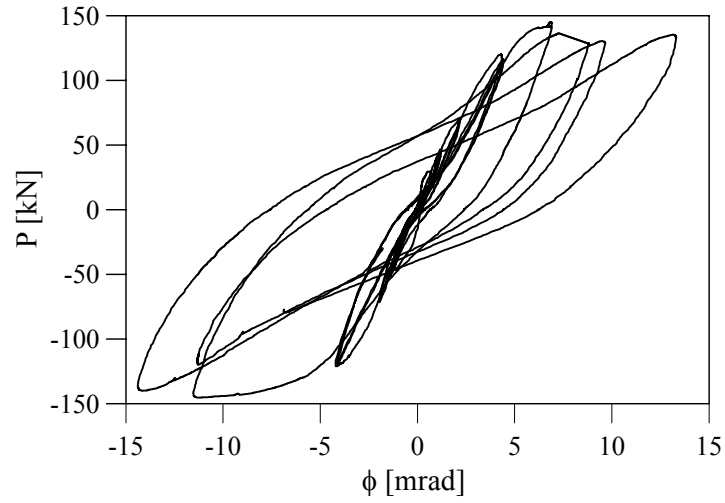


Figure 11. Force-rotation experimental curve for the hybrid joint

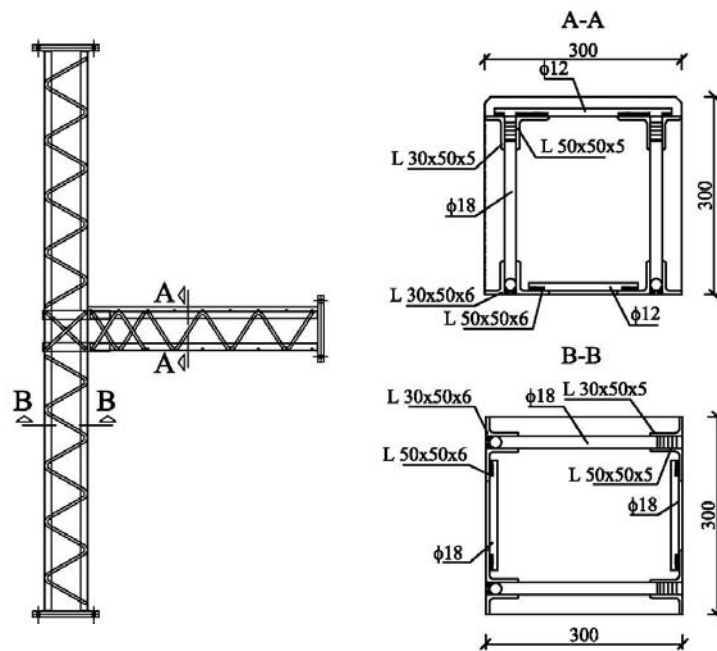


Figure 12. Details of beam-to-column joint analysed in the experimental test



Figure 13. *Damage in the joint under reverse loading*

4. Numerical models

In the research, detailed finite element models have been used to investigate the performance of hybrid elements. Numerical simulations represent a fundamental vehicle to supplement and extend experimental results. They can provide significant information on failure mechanisms, including the distribution of stresses in steel and concrete, which can be used in the formulation of simple analytical models.

The finite element code ABAQUS (ABAQUS, 2004) has been employed for representing the response to collapse of beams A and B and beam-to-column connection. In the accurate 3D models, shell elements have been used for steel angles, beam elements for bars and solid elements for concrete. A rigid connection between concrete and embedded steel was considered, neglecting potential loss of bond. This assumption was confirmed in the experimental tests.

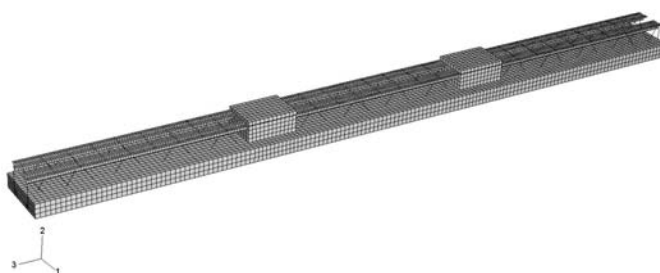


Figure 14. *FE model for the beam type A*

To represent the hybrid members' response to collapse, both material and geometric nonlinearity have been taken into account. In particular, an isotropic elasto-plastic model with hardening, based on the von Mises yield criterion, was

used for steel. While the Concrete Damage Plasticity Model (ABAQUS 2004) was employed to represent the material nonlinearity in concrete, which is assumed as an isotropic continuous material. Such model, which was developed by Lubliner *et al.* (1989) and elaborated later by Lee and Fenves (1998), is based on the classical continuum damage theory, using a modified Drucker-Prager yield function to identify the state of failure and damage. Moreover a non-associated plastic flow rule is employed, thus a plastic potential different from the yield function determines the direction of plastic deformation.

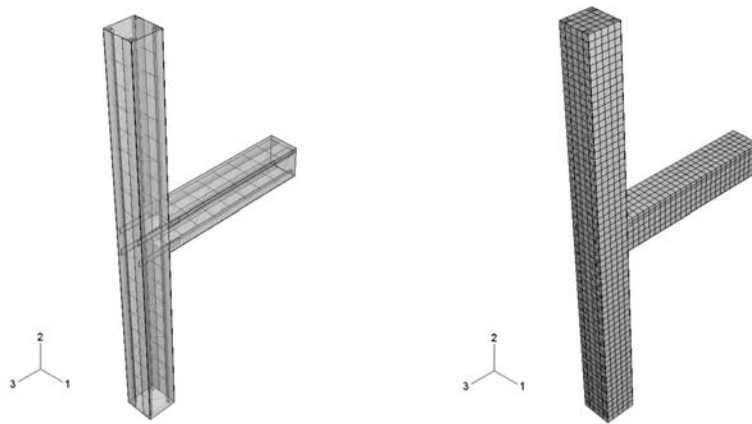


Figure 15. FE model for the beam-to-column connection

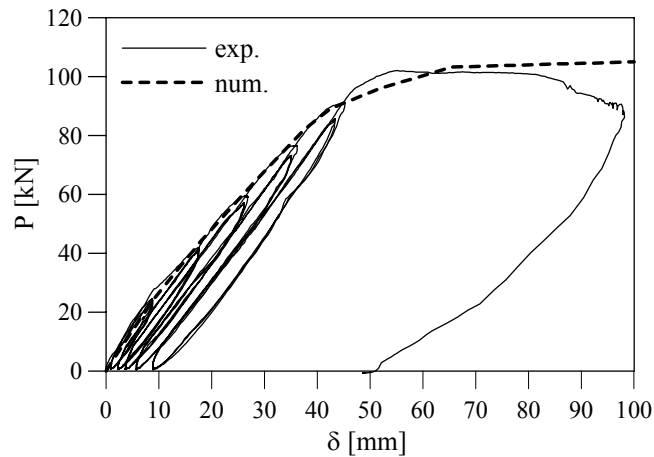


Figure 16. Numerical-experimental comparison on the beam A response

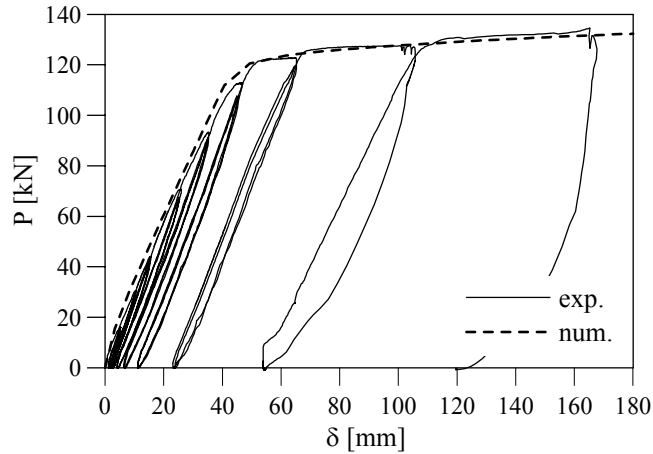


Figure 17. Numerical-experimental comparison on the beam B response

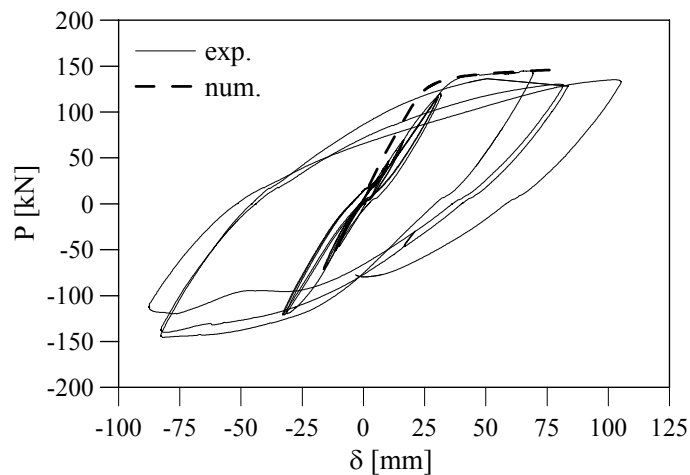


Figure 18. Numerical-experimental comparison on the joint response

The accuracy of FE models for beams and beam-to-column connection (Figures 14-15) has been checked by considering the experimental results achieved in the tests described in previous section. Figures 16-19 show numerical-experimental comparisons, where the numerical curves are obtained assuming monotonic loading condition. Numerical results confirm the ability of the detailed 3D models in representing not only initial stiffness and ultimate capacity of hybrid beams and beam-to-column joint (Figures 16-18), but also strain distribution (Figure 19) and buckling in steel angles (Figure 20). In Figure 19, experimental

curves S.G5 and S.G6 represent strain in the top angles of steel joist, while curves S.G7 and S.G8 indicate the variation of strain in the bottom angles at mid-span. In the experimental test, strains were measured by strain gauges (S.G1-8), which were placed on steel angles and bars as shown in Figure 19.

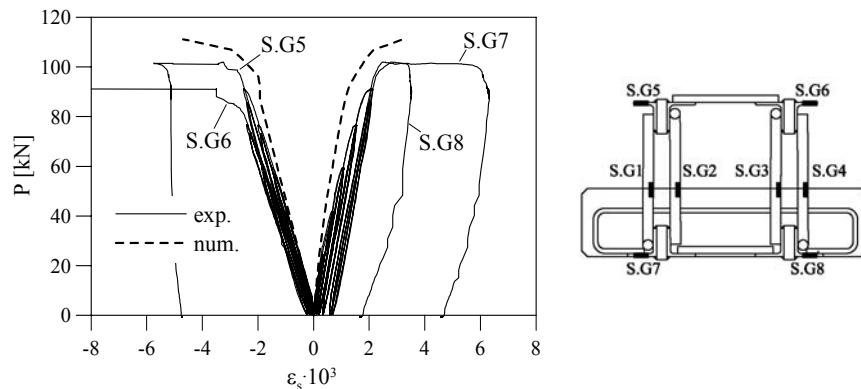


Figure 19. Numerical-experimental comparisons on strain distribution in steel angles of beam A

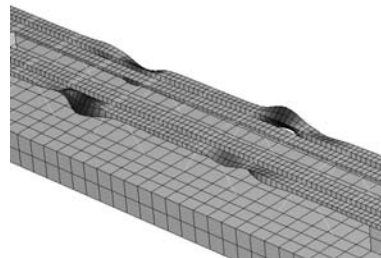


Figure 20. Buckling in steel angles predicted by the detailed FE model

5. Analytical models for structural design

The experimental outcomes and nonlinear numerical simulations have been employed to investigate resistance mechanisms of hybrid elements. In particular, a simple expression for the hybrid member flexural stiffness, which can be used to calculate maximum displacements at serviceability, is proposed, as well as simple analytical models for flexural and shear capacity are provided for beams and beam-to-column joints.

5.1. Beam flexural behaviour

5.1.1. Beam stiffness

The flexural stiffness EJ for beams A and B has been determined as a function of the vertical displacements, which have been measured in the experimental tests or calculated by numerical models at different load levels. Considering the loading arrangement used in the tests (Figure 21) and neglecting shear deformability, the maximum displacement at mid-span δ can be approximated using the relationship:

$$\delta = 0.035 \cdot \frac{Pl^3}{EJ} \quad [1]$$

where P is one of the two symmetric point loads on the beam and l is the span length.

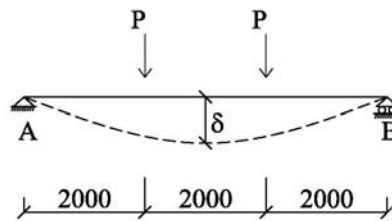


Figure 21. Load arrangement in beams tests (measures in [mm])

An expression for the equivalent flexural stiffness, which accounts for the development of cracks in concrete, can be derived directly from [1]:

$$EJ_{\text{exp(num)}} = 0.035 \cdot \frac{Pl^3}{\delta} \quad [2]$$

Figures 22-23 show the variation of flexural stiffness EJ as a function of the maximum bending moment in the beam M_{max} . The equivalent stiffness has been calculated using [2] and the experimental and numerical values for δ , thus obtaining the curves EJ_{exp} and EJ_{num} respectively. In particular, in the former case, the experimental backbone curve for vertical displacements δ has been considered.

In the figures, two constant values for flexural stiffness, namely EJ_I and EJ_{II} , are shown as well. They can be determined using the traditional transformed section approach and neglecting (uncracked stiffness EJ_I) or considering (cracked stiffness EJ_{II}) cracking in concrete. It can be observed how uncracked and cracked stiffness represent two limit values, which define the most significant interval of variation for EJ .

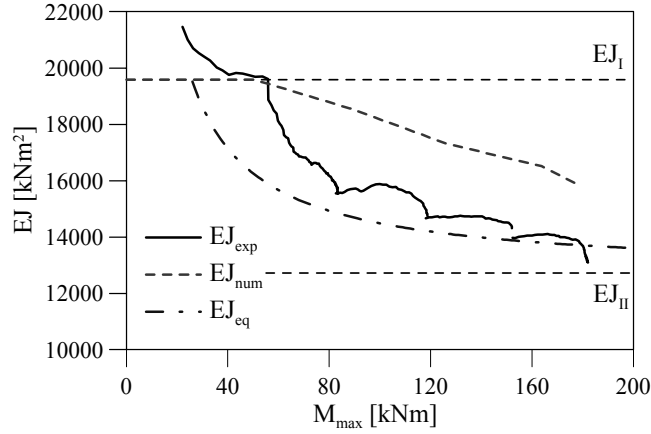


Figure 22. Flexural stiffness for beam type A

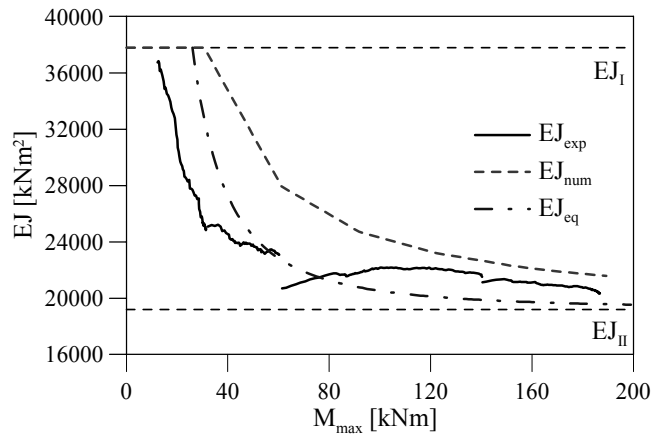


Figure 23. Flexural stiffness for beam type B

In order to define a simple relationship for the variation of EJ_{eq} with the load level, the expression provided by Eurocode 2 (CEN, 2003) can be used. It relates equivalent flexural stiffness to bending moment M in the beam:

$$EJ_{eq} = \begin{cases} EJ_I & \text{when } M \leq M_{crack} \\ \xi EJ_I + (1 - \xi) EJ_{II} & \text{when } M > M_{crack} \end{cases} \quad [3]$$

where $\xi = (M_{crack}/M)^2$ and M_{crack} is equal to the first cracking bending moment.

The values EJ_{eq} defined by [3] is shown in Figures 22-23. They determine, at different load levels, an equivalent flexural stiffness very close to the experimental and numerical values. Therefore [3] can be used for an accurate and practical calculation of hybrid beam displacements.

5.1.2. Beam flexural capacity

Beams A and B are characterized by different flexural resistance. In practical calculations, when designing beams with fully encased steel joists (beam B), the plastic bending capacity can be employed, as plastic deformation is generally reached in steel angles and in concrete under compression. This is mainly because steel components are surrounded and confined by concrete and local buckling is prevented. The effectiveness of using the full plastic capacity in beam design is also confirmed by the analysis of the experimental results for beam B. In this case, the plastic bending resistance $M_{pl} = 225$ kNm, which is calculated ignoring strain hardening, is a safe approximation of the actual ultimate bending moment, which was reached in the four-point load bending test, $M_u = 270$ kNm.

In beams A, only the bottom part of the steel box truss is embedded in concrete, so the top steel angles, which are mainly in compression, can buckle. Therefore, the plastic bending resistance cannot be assumed as a safe estimate of the beam flexural capacity. In this case, the bending resistance M_c can be derived considering the actual buckling mode for the beam, and using the practical formulation provided by Eurocode 3 (CEN, 2005) for buckling resistance of unrestrained members in bending:

$$M_c = \chi \cdot W_y \cdot f_y \quad [4]$$

where W_y is the appropriate section modulus, f_y is the steel yield strength and χ is a reduction buckling factor, which can be calculated considering an imperfection factor $\alpha = 0,49$ (buckling curve c) and the non-dimensional slenderness:

$$\bar{\lambda} = \sqrt{\frac{W_y f_y}{M_{cr}}} \quad [5]$$

where M_{cr} is the elastic critical moment.

When analysing unrestrained steel beams (Eurocode 3, CEN 2005), M_{cr} corresponds to the critical moment for lateral-torsional buckling. Conversely, when considering partially encased hybrid elements, M_{cr} is associated with lateral buckling of the top steel angles only. In this case, a suitable expression for M_{cr} can be obtained as a function of the Euler critical load $N_{cr,E}$ of the top angles. They are laterally restrained by the web diagonal bars, which can be assumed as a continuous system of elastic springs (Figure 24). $N_{cr,E}$ can be then determined employing the relationship provided by Timoshenko and Gere (1961):

$$N_{cr,E} = \frac{\pi^2 EJ}{l^2} \left(m^2 + \frac{\beta l^4}{m^2 \pi^4 EJ} \right) \quad [6]$$

where EJ is the flexural stiffness of the top steel angles, l is the beam length, m is number of half waves at buckling and $\beta = k/a$ is the rigidity of the equivalent continuous elastic system (Figure 24).

When β and m assume high values, as in most of the actual cases, [6] can be approximated by:

$$N_{cr,E} = 2\sqrt{EJ\beta} \quad [7]$$

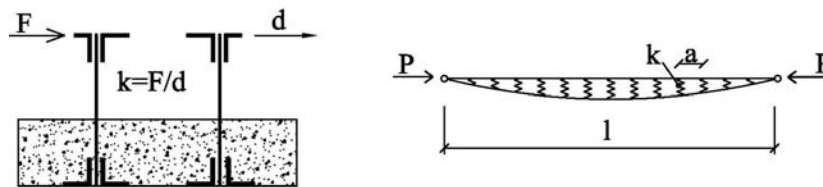


Figure 24. Simple model to account for buckling in top angles

Finally M_{cr} to be used in [5] for hybrid beams type A, is calculated considering the lever arm of internal forces Z :

$$M_{cr} = N_{cr,E} \cdot Z \quad [8]$$

The effectiveness of the analytical model for the flexural capacity of partially encased hybrid beams has been checked by the analysis of beam A. In this case, a bending capacity $M_c = 177$ kNm is calculated using [4] with $\chi = 0.82$, which is derived from $M_{cr} = 730$ kNm ($N_{cr,E} = 2\,920$ kN, $Z = 0.25$ m) and $W_y \cdot f_y = 216$ kNm.

The calculated bending resistance M_c represents a close and safe approximation of the maximum bending moment at collapse $M_u = 204$ kNm, which was determined in the test.

5.2. Shear behaviour of hybrid beams

In order to investigate shear resistance mechanisms for hybrid members, the shear transferred by steel components and reinforced concrete has been identified. The former contribution is mainly associated with the shear capacity and stiffness of steel angles (V_{ang}) and the tensile resistance of the diagonal bars (V_{diag}), while the latter (V_{conc}) is due to the concrete confined in the steel truss. In fact, in the analysed

hybrid elements, as in the case of simple RC members, shear is resisted not only by shear reinforcement, but also through dowel mechanism, aggregate interlock forces and arch action.

To determine analytical formulations for shear capacity, the specific geometric characteristics of hybrid elements and the actual interaction between steel joist and RC member have been taken into account. The steel box truss alone and beams type A and B have been analysed by means of numerical simulations to collapse. The same cross section for steel joists and hybrid elements used in experimental tests, as well as the same material properties have been assumed in all the analyses. In particular, two sets of beams, characterized by different span length and loading arrangement, have been investigated. Each group of beams includes a steel box truss, a beam A and a beam type B. In the first set, the same span length ($L = 6$ m) as well as the same load arrangement used in the experimental tests have been considered. While in the second set, shorter beams with a span length $L = 2$ m, which fail because of shear under three-point load, have been analysed.

5.2.1. Numerical analyses

In the FE model for the steel joist, material nonlinearity has been considered, while second order effects have been neglected. This is because the aim of these simulations is to determine stress distribution in the steel components which transfer shear, considering the same conditions found in the case of beams type A and B. Therefore local buckling in diagonal bars in compression must be ignored as, in real hybrid elements, it is prevented by surrounding concrete.

At different loading level and for each analysed beam, the resistance contribution associated with diagonal bars can be determined using the normal stress in the bars through the expression:

$$V_{diag} = \sigma_d \cdot A_d \cdot n_d \cdot \sin \alpha \quad [9]$$

where σ_d represents the mean stress in the diagonal element, which is calculated through the numerical simulation, A_d is the diagonal cross section area, n_d is the number of diagonal elements in the same section and α corresponds to the inclination of the diagonal bars.

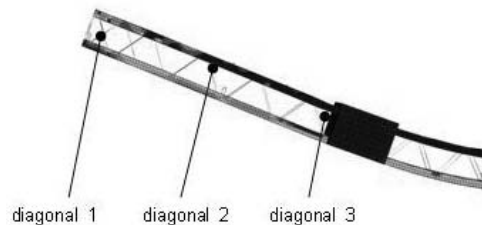


Figure 25. Diagonal bars in half model for the first set of beams

The diagonal bars contribution in steel joist and beams A and B is shown in Figures 26-30. All the results presented refer to three specific beam sections, which are placed at 0.1 m, 0.8 m, and 1.8 m from the lateral support and are associated with the normal stress in diagonal 1, 2 and 3 shown in Figure 25.

Considering the numerical results on the behaviour of steel joist, the portion of shear transferred by the angles V_{ang} has been calculated subtracting the diagonal bars contribution [9], named shear diagonal, from the total shear V_{tot} .

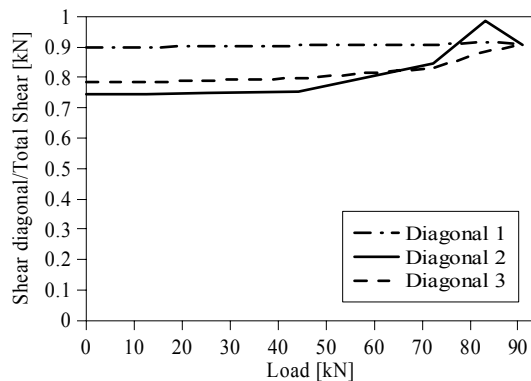


Figure 26. Shear transferred by the web diagonal bars of the steel joist at different load levels

The ratio between the shear transferred by web bars and total shear, at different loading level, is displayed in Figure 26. It can be observed that diagonal elements resist most of the shear (about 80-90% of total shear), thus the contribution of steel angles is limited (about 10-20% of the total shear). By increasing the load level, the fraction of total shear transferred by diagonal bars varies. This is caused by the development of material nonlinearity in the beam components, steel angles and bars.

In the analysis of beams A and B, the contribution associated with the bottom RC has been considered as well. Figures 27-29 display the portion of total shear transferred by diagonal bars at different load levels, while Figures 28-30 shows the variation of the different contributions (diagonal bars, steel angle and concrete) at collapse, along one-third of the beams length from the support. In all the cases, the contribution due to concrete, V_{conc} , has been obtained by subtracting from the total shear, the portions transferred by diagonal bars and steel angles. In particular, V_{diag} has been derived from [9], using the σ_u values obtained from hybrid beams FE analyses. While V_{ang} has been calculated considering a ratio $V_{ang}/V_{diag} = 0.11$, which corresponds the value found in the analysis of steel joist at collapse (Figure 26), when large plastic deformations occur in bars and angles. This is an approximation as V_{diag}/V_{ang} varies with the load level. However this variation is very limited (Figure 26), so the ratio $V_{diag}/V_{ang} = 0.11$ can be assumed in evaluating shear resistant contributions for hybrid members.

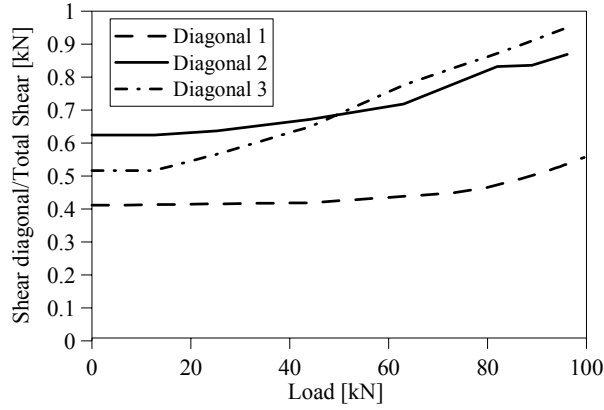


Figure 27. Shear transferred by the web diagonal bars of beam type A at different load levels

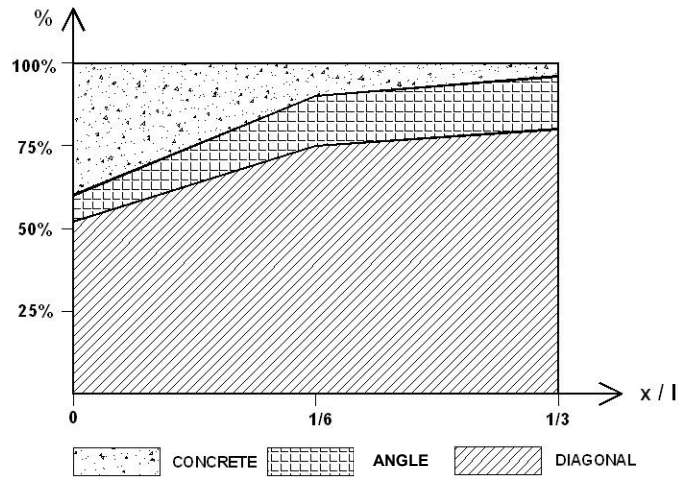


Figure 28. Variation of different resistance contributions along one-third of the beam A length

Figures 27-28 show that the shear resistance provided by concrete is not negligible, even in the case of beam A, where only a bottom RC member is connected to steel joist. It is particularly relevant along the whole beam at low load levels, as it can be observed by comparing the ratio of shear transferred by steel diagonal bars shown in Figures 26 and 27. Conversely, at collapse, the concrete contribution is significant (about 40% of total shear) only close to the support, where concrete is uncracked, because of the low bending moment (Figure 28).

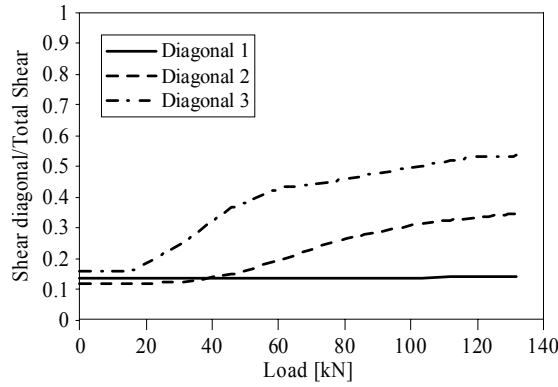


Figure 29. Shear transferred by the web diagonal bars of beam type B at different load levels

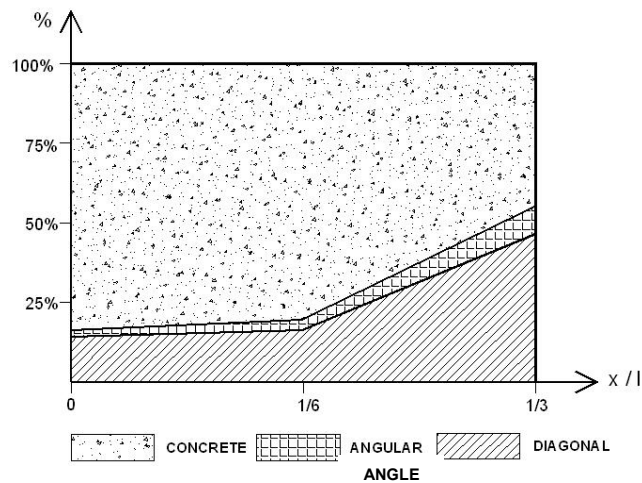


Figure 30. Variation of different resistance contributions along one-third of the beam B length

A much higher concrete shear contribution characterizes the shear capacity of beam type B (Figures 29-30), evidently because the steel joist is fully embedded in RC. In this case, at collapse, about 80% of total shear is transferred by concrete close to the support, and about 50% at maximum bending moment.

Similar results have been achieved in the analyses of the shorter beams under three-point load. They are summarized in Table 2, where the shear at failure V_{us} , together with the shear contribution transferred by concrete steel diagonal bars and angles, are shown.

Table 2. Shear capacity for the second set of beams

	V_u [kN]	V_{conc}/V_u [%]	V_{diag}/V_u [%]	V_{ang}/V_u [%]
Steel joist	198	/	86	14
Beam A	263	25	65	10
Beam B	336	41	51	8

The results for the steel joist and for beam type B are equivalent to those obtained in the first group of beams. Conversely, in the case of beam A, the contribution of concrete is higher for the shorter beam, as cracking due to bending is very limited.

5.2.2. Analytical models for shear resistance

The accuracy and effectiveness of two different models for shear resistance have been checked using the results of the numerical simulations on hybrid beams, which are described in the previous section. In particular, the numerical outcomes achieved in the analysis of the shorter beams have been considered, as they refer to a *quasi*-pure shear failure, where the influence of the flexural behaviour can be ignored.

In the case of fully encased hybrid beams (beam B), two alternative formulations are proposed: shear model 1 and model 2. Both of them consider the analogy between shear capacity of hybrid section and resistance of a parallel chord truss, which was postulated by Morsch for RC members.

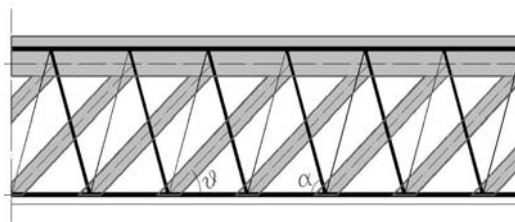


Figure 31. Truss mechanism used in the shear model 1 for fully encased hybrid beams

In shear model 1, the beam is represented by a truss (Figure 31), which follows the geometry of the steel joist embedded in RC. It consists of two parallel chords, which are connected each other by means of the diagonal web reinforcement ($\alpha = 54^\circ$) resisting tension, and concrete struts withstanding compression forces. The inclination of concrete struts ($\beta = 33^\circ$) can be determined considering the

intersection of steel diagonal elements with the top concrete chord in compression (Figure 31). According to this model, shear failure is reached when internal forces in the web components of the truss exceed either the tensile strength of diagonal bars or the compressive capacity of concrete strut. The formulation is similar to that currently employed for RC members, so the shear strength relationships, provided by Eurocode 2 (CEN, 2003) for members with shear reinforcement, can be used:

$$V_{Rcd} = 0.9b \cdot d \cdot \nu \cdot \sigma_{cd} \cdot \sin^2 \vartheta \cdot (\cot \alpha + \cot \vartheta) \quad [10]$$

$$V_{Rsd} = A_{sw} \cdot f_{yd} \frac{0.9 \cdot d}{s} \cdot \sin \alpha \cdot (\cot \alpha + \cot \vartheta) \quad [11]$$

where V_{Rcd} refers to the capacity of concrete, while V_{Rsd} corresponds to the web reinforcement resistance, b and d are width and effective depth of the cross-section, σ_{cd} is the design concrete compressive strength, ν is a factor accounting for the actual stress distribution along the concrete strut ($\nu = 0.5$), A_{sw} represents the area of steel shear reinforcement, s is the diagonal bars spacing and f_{yd} is the steel yield strength. According to model 1, the shear capacity of the hybrid section is equal to the lesser of V_{Rcd} and V_{Rsd} .

In the model 2, the resistance of two different mechanisms, assumed to act in parallel, are added to determine the hybrid section shear capacity. The first contribution, $V_{R,conc}$, refers to the shear strength of the concrete web without shear reinforcement (Eurocode 2, CEN 2003), which is confined by the steel box. The latter, $V_{R,diag}$, can be calculated considering the truss displayed in Figure 32, where a top concrete chord is connected to the bottom steel angles by means of the steel diagonal bars, which resist both tensile and compressive forces. It is assumed that concrete prevents buckling of the diagonal bars under compression, but its resistance contribution is not directly considered in the truss model.

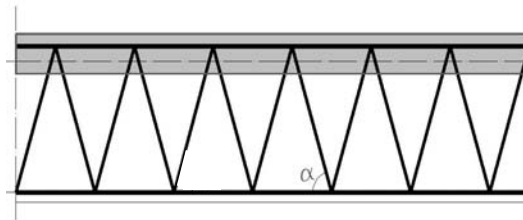


Figure 32. Truss mechanism used in the shear model 2 for fully encased hybrid beams

$$V_{Rd} = V_{R,diag} + V_{R,conc} \quad [12]$$

with:

$$V_{R,diag} = A_{sw} \cdot f_{yd} \cdot s \cdot n \alpha \quad [13]$$

$$V_{R,coc} = [C_{Rd,c} \cdot k (100\rho_l \cdot f_{ck})^{1/3}] b_w \cdot d \quad [14]$$

where, according to Eurocode 2 (CEN, 2003): $C_{Rd,c}$ is the concrete basic shear strength, which is assumed $C_{Rd,c} = 0.18/\gamma_c$, k is a coefficient which accounts for the effectiveness of aggregates interlocking as a function of the effective depth of the cross-section d , $k = 1 + \sqrt{200/d} \leq 2$, ρ_l represents the amount of longitudinal steel reinforcement ($\rho_l = A_{sl}/b_w \cdot d \leq 0.02$), and f_{ck} is the concrete compressive strength.

Table 3. Comparisons on shear resistance of the second set beam type B

	FE model	Shear model 1	Shear model 2
V_{diag} [kN]	171	239	171
V_{ang} [kN]	27	/	/
V_{conc} [kN]	138	492	58
$V_{Rd}(V_u)$ [kN]	336	239	229

Table 4. Comparisons on shear resistance of the second set beam type A

	FE model	Shear model 2
V_{diag} [kN]	171	171
V_{ang} [kN]	27	/
V_{conc} [kN]	65	77
$V_{Rd}(V_u)$ [kN]	263	248

In the case of partially encased hybrid sections (beam type A), only model 2 can be used for determining shear resistance, accounting for buckling of the diagonal bars. In fact, as the top chord of the steel box truss is not embedded in concrete, a truss mechanism with concrete diagonal struts (shear model 1 above) is not realistic, and cannot be used for representing the shear capacity. In Tables 3 and 4, the shear resistance obtained using shear model 1 and 2 in the case of beam type B and only model 2 for beam A, are compared against the ultimate shear capacities (V_u), which have been determined in the nonlinear numerical simulations. The results achieved

show that either shear model represents a safe approximation of ultimate shear and can be used in practical design for hybrid fully-encased beams. In the case of beam type A, model 2 provides a suitable value for the shear resistance, close to the numerical value. However, when designing hybrid partially-encased beams, it is suggested to consider only the contribution provided by diagonal bars, neglecting, for the sake of safety, the resistance of the shear mechanism with concrete ($V_{R,conc} = 0$).

5.3. Beam-to-column joint

The performance of beam-to-column connections in hybrid frames, relies on the ability of the joint steel truss and concrete to withstand shear forces. The specific arrangement of steel reinforcement in the joint, which includes four plates welded to the steel angles of the columns, and four diagonal bars (Figure 33), provides confinement to the concrete, ensuring effective combined resistance mechanisms.

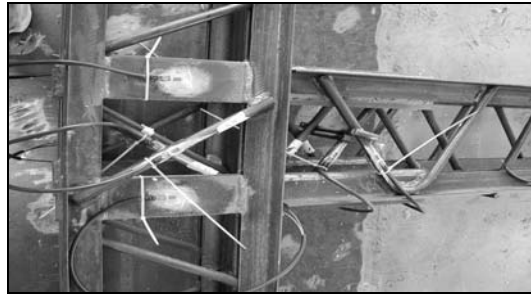


Figure 33. Details of reinforcement for external joints in hybrid frames

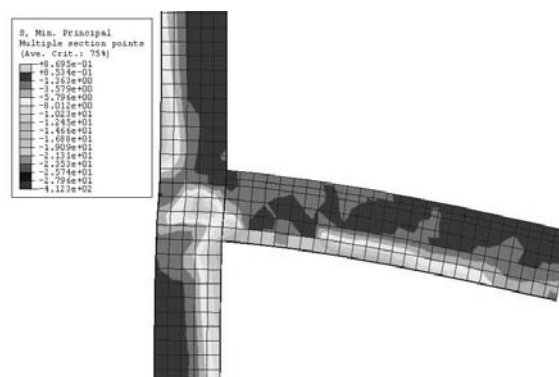


Figure 34. Maximum principal stress (compression) in concrete at maximum load

This is confirmed by the outcomes of the numerical simulations, which have been carried out to investigate the response to collapse of the external joint analysed in the experimental test. Figures 34-35 show high stress values in concrete and steel at the maximum load reached in the test, thus revealing how both confined concrete and steel reinforcement are effectively exploited to transfer bending and shear force from the beam to the column. Highest stress values have been found not at the joint, but at the end of the beam, where, according to the design assumptions, a plastic hinge forms.

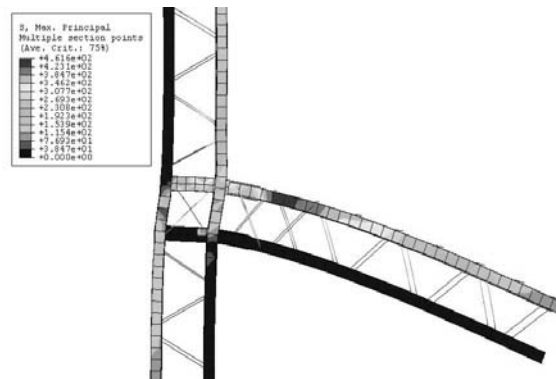


Figure 35. Maximum principal stress in steel components at maximum load

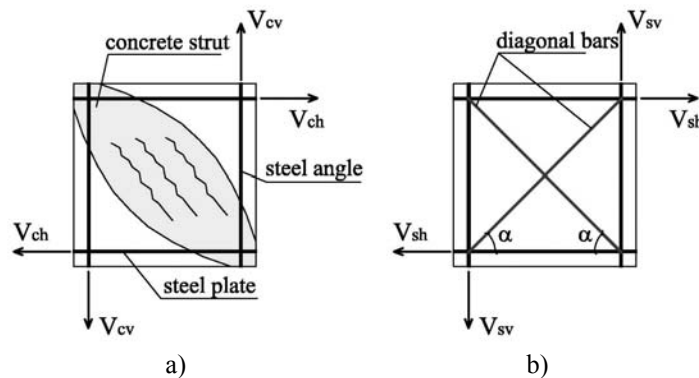


Figure 36. Resistance mechanism for beam-to-column connection

Two resistance mechanisms, which act in parallel, can be clearly identified to represent the shear capacity of the joint. The former, which is characteristic of RC joints (Park and Paulay, 1975), is associated with a concrete diagonal strut

(Figure 36a), while the latter is due to the joint reinforcement (Figure 36b). In practical calculations, the shear capacity of the joint can be evaluated considering the horizontal components of the resistance force, which correspond to V_{ch} for the concrete strut and V_{sh} for the steel reinforcement contribution (Figures 36a, 36b).

The shear resistance of the joint is then calculated using the relationship:

$$V_{Rd,j} = V_{Rj,steel} + V_{Rj,conc} \quad [15]$$

where $V_{Rj,conc}$ ($= V_{ch}$) and $V_{Rj,steel}$ ($= V_{sh}$) represent the resistance of concrete strut and steel diagonal bars respectively. The concrete contribution is associated with the shear capacity of plain concrete members (Eurocode 2, CEN 2003):

$$V_{Rj,conc} = C \cdot \frac{0.25 \cdot f_{ck}}{\gamma_c} \cdot b_j \cdot h_j \quad [16]$$

with $C = 15$ for external joints and $C = 20$ for external beam-to-column connections, while b_j and h_j are the joint width and beam depth respectively. The shear resistance provided by the joint steel reinforcement is given by:

$$V_{Rj,steel} = n_{diag} \cdot A_d \cdot f_{yd} \cdot \cos \alpha \quad [17]$$

where n_{diag} corresponds to the number of diagonal elements in the joint, A_d is the section area of each bar, while α is the bar inclination with respect to the horizontal plane (Figure 36b).

Using [16] and [17] to calculate the resistance associated with the two mechanisms, the following values have been determined: $V_{Rj,conc} = 450$ kN, $V_{Rj,steel} = 314$ kN. Thus, according to [15], $V_{Rd,j} = 764$ kN, which is higher than the maximum load achieved in the test: $V_u = 670$ kN. This is because V_u was reached at the failure of the beam, which was designed to resist bending and shear force lower than the capacity of the joint.

In order to guarantee an adequate joint response under cyclic loading, stresses in the joint region should be limited by specific values. The stress state in the beam-to-column connection can be determined by considering internal forces at the end of column or beam. Thus, given axial and shear force at the end of the column, N_c and V_c , normal and shear stress in the joint (σ_j and τ_j) can be easily calculated by means of the relationships:

$$\sigma_j = \frac{N_c}{b_j \cdot h_{jc}} \quad \text{and} \quad \tau_j = \frac{V_c}{b_j \cdot h_{jc}} \quad [18]$$

where h_{jc} is the depth of the confined concrete section in the joint, which corresponds to the distance between the pairs of column angles. The principal stress values can be calculated using the Mohr assumptions, thus achieving:

$$\sigma_{\eta} = \sqrt{\left(\frac{\sigma}{2}\right)^2 + \tau^2} + \frac{\sigma}{2} \quad \text{and} \quad \sigma_{\xi} = \sqrt{\left(\frac{\sigma}{2}\right)^2 + \tau^2} - \frac{\sigma}{2} \quad [19]$$

with σ_{η} maximum stress in compression and σ_{ξ} maximum tensile stress.

To assure adequate joint performance, the maximum stresses must be lower than specific limit values, which indicate the onset of significant damage and cracks in the joint region. According to (NTC 2008), the maximum compressive and tensile stress, σ_{η} and σ_{ξ} , must satisfy the following relationships:

$$\sigma_{\eta} \leq \eta \cdot f_{cd} \quad [20]$$

which, according to [19], leads to:

$$\tau \leq \eta \cdot f_{cd} \sqrt{1 - \frac{v_d}{\eta}} \quad \text{with} \quad v_d = \frac{\sigma}{f_{cd}} \quad [21]$$

and

$$\sigma_{\xi} \leq f_{ctd} \quad [20]$$

which corresponds to:

$$\tau \leq f_{ctd} \sqrt{1 + \frac{\sigma}{f_{ctd}}} \quad [22]$$

where f_{cd} and f_{ctd} are the concrete design compressive and tensile strength, while η is a reduction factor, which considers the interaction between tensile and compressive principal stresses and it is given by:

$$\eta = \alpha_j \left(1 - \frac{f_{ck}}{250}\right) \quad [23]$$

with $\alpha_j = 0.6$ for interior joints and $\alpha_j = 0.48$ for exterior joints.

When specific reinforcement is employed to provide higher confinement to concrete, the confinement stress σ_{conf} can be calculated using the expression:

$$\sigma_{conf} = \frac{A_{sh} \cdot f_{yd}}{b_j \cdot h_{jw}} \quad [24]$$

where A_{sh} is the confinement reinforcement area and h_{jw} is the distance between the two pairs of steel angles in the beam. The confinement stress provided by additional steel reinforcement modifies the stress state in the joint, thus leading to:

$$\sigma_{\xi} = \sqrt{\left(\frac{\sigma - \sigma_{conf}}{2}\right)^2 + \tau^2} - \frac{\sigma + \sigma_{conf}}{2} \quad [25]$$

Again the maximum tensile stress σ_{ξ} must be less than concrete tensile strength, which gives:

$$\sigma_{conf} \geq \frac{\tau^2}{f_{ctd} + \sigma} - f_{ctd} \quad [26]$$

which is equivalent to:

$$\frac{A_{sh} \cdot f_{yd}}{b_j \cdot h_{jw}} \geq \frac{(V_c / b_j h_{jc})^2}{f_{ctd} + v_d f_{cd}} - f_{ctd} \quad [27]$$

Therefore, when designing beam-to-column joints in hybrid frames, two main checks must be considered. They refer to i) the maximum compressive stress in the concrete strut, which must be less than the concrete compressive strength reduced by η factor [21], ii) the minimum amount of confinement provided by reinforcement to concrete [27], which prevents the development of large cracks in tension.

6. Conclusion

In the paper, a new structural system with RC-encased steel joist beams and columns has been investigated. Using the results of experimental tests and numerical simulations, which have been carried out using advanced 3D nonlinear models, the main resistance mechanisms for beams and beam-to-column joints have been determined. Simple analytical models have been suggested to represent the flexural and shear behaviour of beam and the capacity of exterior joints. In particular, a relationship for flexural stiffness of hybrid beams, to be used when calculating the maximum displacements at serviceability, has been defined. Analytical models for the bending resistance of partially and fully-encased steel joist beams have been proposed as well. They refer to the capacity of the hybrid beams during the construction, before the hardening of the cast-in-place concrete, and to the behaviour at Ultimate Limit State. In the first case, it was found that the flexural resistance depends on the buckling of the top steel chord, while, in the second case, the full plastic capacity of the composite cross section can be exploited. Concerning the shear resistance, two alternative models have been proposed for hybrid beams. The former is based on a composite truss mechanism with steel web diagonal reinforcement and concrete struts. While, in the latter, the resistance provided by a truss with steel web components is added to the shear resistance of an equivalent RC concrete cross section without shear reinforcement. Finally, with reference to the joint behaviour, simple rules are provided for determining the shear capacity and

limiting maximum stresses in the joint regions, so as to assure adequate performance even in the case of cyclic loading. The proposed analytical models for beams and joints, which provide a safe estimate of the structural response, can be effectively used when designing hybrid frames.

7. References

- ABAQUS, *User's Manual*, Version 6.5.1, Hibbitt, Karlsson and Sorensen, Pawtucket, RI, USA, 2004.
- Amadio C., Macorini L., Suraci G., "Structural performance of a new hybrid RC-encased steel joist system", *Advanced in Reinforced Concrete and Precast Constructions*, Ed. Marco di Prisco, Starrylink Editrice, December 2008, Milan, Ital, p. 19-29.
- CEN, EN 1992-1-1, *Eurocode 2, Design of concrete structures - Part 1-1: General rules and rules for buildings*, Brussels, 2003.
- CEN, EN 1993-1-1, *Eurocode 3, Design of steel structures Part 1-1: General rules and rules for buildings*, Brussels, 2005.
- Hsu H.L., Hsieh J.C., Juang J.L., "Seismic performance of steel-encased composite members with strengthening cross-inclined bars", *Journal of Constructional Steel Research*, Vol. 60, 2004, pp. 1663-1679.
- Johnson R. P., *Composite structures of steel and concrete, Volume 1: beams, slabs, columns and frames for buildings*, London, Blackwell Scientific Publication, 1994.
- Ju Y. K., Kim J.Y., Kim S.D., "Experimental evaluation of new concrete encased steel composite beam to steel column joint", *Journal of Structural Engineering ASCE*, Vol. 133, No. 4, 2007, p. 519-529.
- Khuntia M., Goel S.C., "Experimental study of FRC-encased steel joist composite beams", *Journal of Structural Engineering ASCE*, Vol. 125, No. 5, 1999, p. 495-501.
- Khuntia M., Goel S.C., "Analytical study of FRC-encased steel joist composite beams", *Journal of Structural Engineering, ASCE*, Vol. 125, No. 5, 1999, p. 503-509.
- Lubliner J., Oliver J., Oller S., Onate E., "Plastic-damage model for concrete", *International Journal of Solids and Structures*, Vol. 25, No. 3, 1989, p. 299-329.
- Lee J., Fenves G.L., "Plastic-damage model for cyclic loading of concrete structures", *Journal of Engineering Mechanics, ASCE*, Vol. 124, No. 8, 1998, p. 892-900.
- Mullett D. L., *Composite floor systems*, The Steel Construction Institute, Blackwell Science, UK, 1998.
- Naccarato P. A., "Low floor-to-floor heights", *Modern Steel Construction*, American Institute of Steel Construction, 2000.
- NTC, *Nuove norme tecniche per le costruzioni*, Decreto Ministeriale 14/1/2008, Italy, 2008.
- Park R., Paulay T., *Reinforced Concrete Structures*, John Wiley & Sons, 1975.

Parra-Montesinos G. J., Dasgupta P., Goel S.C., “ Development of connection between steel truss-FRC beams and RC columns for precast earthquake-resistant framed construction”, *Engineering Structures*, Vol. 27, 2005, p. 1931-1941.

Timoshenko S. P., Gere J. M., *Theory of Elastic Stability*, McGraw-Hill, New York, USA, second edition, 1961.

Received: 26 April 2011

Accepted: 19 September 2011